Journal of Materials Chemistry A

Accepted Manuscript

This is an *Accepted Manuscript*, which has been through the Royal Society of Chemistry peer review process and has been accepted for publication.

Accepted Manuscripts are published online shortly after acceptance, before technical editing, formatting and proof reading. Using this free service, authors can make their results available to the community, in citable form, before we publish the edited article. We will replace this *Accepted Manuscript* with the edited and formatted *Advance Article* as soon as it is available.

You can find more information about *Accepted Manuscripts* in the Information for Authors.

Please note that technical editing may introduce minor changes to the text and/or graphics, which may alter content. The journal's standard Terms & Conditions and the Ethical guidelines still apply. In no event shall the Royal Society of Chemistry be held responsible for any errors or omissions in this *Accepted Manuscript* or any consequences arising from the use of any information it contains.

ROYAL SOCIETY OF CHEMISTRY

www.rsc.org/materialsA

Cite this: DOI: 10.1039/c0xx00000x

www.rsc.org/xxxxxx

ARTICLE TYPE

Synthesis of cadmium sulfide quantum dot-decorated barium stannate nanowires for photoelectrochemical water splitting†

Zemin Zhang,‡[a] Xiaodong Li,‡[b] Caitian Gao,[a] Feng Teng,[a] Youqing Wang,[a] Lulu Chen,[a] Weihua Han,*[a] Zhenxing Zhang[a] and Erqing Xie*[a]

Received (in XXX, XXX) XthXXXXXXXXX 20XX, Accepted Xth XXXXXXXXX 20XX
DOI: 10.1039/b000000x

We report the fabrication of cadmium sulfide (CdS) quantum dot-decorated barium stannate ($BaSnO_3$) nanowires and their application as photoanode for photoelectrochemical water splitting. First, polycrystalline $BaSnO_3$ nanowires, which have a perovskite structure, were prepared by electrospinning their polyvinylpyrrolidone polymer precursors and calcining the resultant polymer fibres. Then, CdS quantum dots were decorated onto the $BaSnO_3$ nanowires with a wet-chemical method. Our results show that the hybrid photoanode made of the CdS quantum dot-decorated $BaSnO_3$ nanowires exhibits a high photocurrent density up to 4.8 mA cm^{-2} at 0 V (*vs.* saturated calomel electrode), which corresponds to a hydrogen generation rate of 71.8 μmol $(h\ cm^2)^{-1}$ with a Faradaic efficiency of around 80%. Its favourable performance was attributed to the effective charge separation at the type II staggered gap heterojunction formed at the $BaSnO_3$/CdS interface, and the low charge recombination in $BaSnO_3$ nanowires during transport. Our findings indicate that the water splitting performance of photoelectrochemical cells can be highly improved by rationally building a type II band alignment heterojunction with sensitizing quantum dots and wide band gap semiconductor nanowires which have a low charge recombination rate during transport.

1. Introduction

Solar-driven water-splitting with photoelectrochemical (PEC) cells is a promising approach to convert solar energy into storable hydrogen (H_2) fuel in an environment friendly manner.[1-4] Generally, PEC water-splitting occurs in three steps: the generation of electron-hole pairs excited by the photons, the migration of photo-excited carriers to the active sites on electrode surface and the redox of water to generate hydrogen and oxygen.[5, 6] Obviously, the amount of photo-excited carriers which can reach the active sites on the surface and participate the redox reaction will vitally determine the ultimate energy conversion efficiency. Significant efforts have been devoted to finding new photoanode materials which can effectively generate and transfer the photo-excited carriers to the active sites[7-10] since its first discovery by Honda and Fujishima in 1972.[11]

Among all these attempts, building a type-II staggered gap heterojunction structure[8] in which one material's conduction band and valance band are more negative than the other ones, is deemed as a potential solution to increase the generation rate of photo-excited carriers.[10] In such a structure, photo-excited electrons will flow to the lower conduction band, while the holes will go into the other materials which have a higher valence band and lower overall hole energy.[12-23] It works like a PN solar cell and predictably leads to a high electron-hole separation rate. Moreover, the type II band heterojunction made of two materials, which has two band gaps and allows capturing two lights, is believed to have a higher energy utilizing efficiency compare with single light absorber.[14, 21-24]

Another issue that limits the energy conversion efficiency of PECs from practical application is the carrier's recombination that undergoes all the water splitting process. Effective water splitting requires a successful carrier transfer from the photocarrier generation location to the active sites where the redox reaction occurs on the photoelectrode. From this point, photoanode materials which have a high carrier mobility and long life time are preferred for water splitting.[14, 25]

As alternative PEC photoanode materials, ternary oxide semiconductors are better candidates than binary oxides, due to their tuneable properties by altering their chemical composition.[26] Among the reported ternary oxide photoanode materials, $BaSnO_3$ has gathered much more attentions for the potential application as working electrode material of PEC device. $BaSnO_3$ is an n-type semiconductor with a band gap of 3.1 eV. The conduction band edge potential of $BaSnO_3$ is 0.69 V negative than normal hydrogen electrode, which is very suitable for electron transfer from $BaSnO_3$ to electrolyte.[27]

In this work, $BaSnO_3$ nanowires (NWs) and CdS quantum dots (QDs) were selected to build a type-II heterojunction which facilitates an effective charge separation. Benefited by the high charge separation rate, lower charge recombination rate in $BaSnO_3$ and effective visible light absorption of CdS QDs, the CdS QD-decorated $BaSnO_3$ NWs photoanode exhibits a high photocurrent density up to 4.8 mA cm^{-2} at 0 V(vs. saturated

Journal of Materials Chemistry A Accepted Manuscript

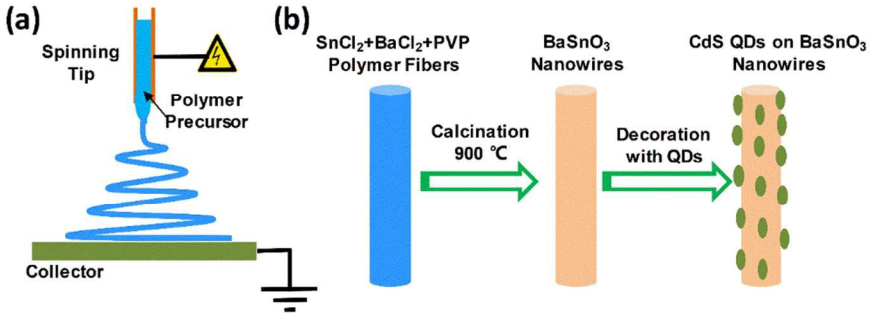

Fig. 1 Fabrication process of the CdS QD-decorated $BaSnO_3$ NWs. (a) electrospin PVP/$SnCl_2$/$BaCl_2$ polymer fibers, (b) calcinate the polymer fibers to obtain $BaSnO_3$ NWs and then decorate CdS QDs onto the $BaSnO_3$ NWs.

calomel electrode), which corresponds to a hydrogen generation rate of 71.8 μmol (h cm^2)$^{-1}$ with a Faradaic efficiency of around 80%. The $BaSnO_3$ NWs were fabricated with a facile electrospinning method associated with a calcination process. CdS QDs were decorated onto the NWs with a wet-chemical method.

2. Experimental

The scheme in Fig. 1 illustrates the experimental procedures for the preparation of CdS QD-decorated $BaSnO_3$ NWs. Firstly, polymer fibres consisted of PVP, $BaCl_2$ and $SnCl_2$ were prepared with a facile electrospinning method. $BaSnO_3$ NWs were formed after a calcination process to remove the organic polymer. Then, CdS QDs were decorated onto the NWs with a wet-chemical method.

2.1. Synthesis of the $BaSnO_3$ NWs

The miscible solvent used in this work is a mixture of conventional solvents containing ethanol, N, N-dimethyl formamide (DMF), acetic acid and deionized water with a mass ratio of 3:4:2:3. Firstly, ethanol, N, N-dimethyl formamide (DMF) and acetic acid were mixed together with the afore-mentioned mass ratio. Then 0.158 g tin dichloride dehydrate ($SnCl_2$•$2H_2O$, Tianjin Chemical Corp, China) was dissolved in 4.5 g mixture obtained previously and stirred for 30 min at room temperature on a magnetic stirring stage. Secondly, 1.5 g deionized water and 0.171 g barium chloride dehydrate ($BaCl_2$ • $2H_2O$, Chengdu Kelong chemical Corp, China) were added into the solution and then stirred for another 30 min. Thirdly, various amount of polyvinylpyrrolidone (PVP, Sigma Aldrich, Mw = 1, 300, 000) was added into the resultant solution and vigorously stirred for 4 h at ambient temperature. Three typical weight ratios, 9%, 11% and 13% between PVP and the solution were selected in our experiment.

In the electro-spinning process, the high voltage and needle-to-collector distance were 20 kV and 20 cm, respectively. The flow rate of the polymer solution used here was fixed at 0.6 mL h^{-1} in all the experiments. The electrospun fibres were collected on an aluminium foil.

The as-spun products were transferred to an alundum boat and calcinated at 900 °C for 2 h in the air to remove the polymer with a temperature increasing rate of 2 °C min^{-1}.

2.2. $BaSnO_3$ NWs coated onto transparent substrates

The obtained $BaSnO_3$ NWs (0.02 g) were ultrasonically dispersed in a mixture of 0.34 g deionized water, 0.067 g ethanol and 0.817 g acetic acid. Then, 0.015 g polyethylene glycol (PEG, Mw = 20 000) was added into the above solution and vigorously stirred for 1 h at ambient temperature. The paste was drop-coated onto F-doped tin oxide glasses (FTO, 2.2 mm in thickness, >90% transmittance, 14 Ω per square, Nippon, China).[28] The films were then annealed at 500 °C for 2 h with a temperature increasing rate of 2 °C min^{-1}.

2.3. CdS QDs decoration

The CdS QDs were decorated onto the $BaSnO_3$ NWs with a successive ionic layer adsorption and reaction (SILAR) method.[22] Briefly, the samples ($BaSnO_3$ NW coated FTO) were successively immersed into $Cd(NO_3)_2$ aqueous solution (0.05 M) for 4 min, DI water for 30 sec, Na_2S aqueous solution (0.05 M) for 4 min and DI water for 30 sec again. The entire four-step procedure is one SILAR cycle. The desired amount of CdS QDs was obtained by controlling the running cycles. Finally, the films were annealed at 400 °C for 30 min in the air.

2.4. Characterization

The morphology of the CdS-decorated $BaSnO_3$ NWs were investigated by a field emission scanning electron microscope (FE-SEM, Hitachi S-4800), and high-resolution transmission electron microscope (HRTEM, FEI Tecnai F30). Elemental analysis was performed on an X-ray photoelectron spectroscope (XPS), which is carried out on a Kratos AXIS Ultra DLD XPS instrument equipped with an Al Kα source. An energy-dispersive X-ray (EDX) spectroscopy equipped to the TEM (*in-situ*) is also performed to confirm their chemical compositions. X-ray diffraction (XRD, Philips, X'per pro, Cu kα) is employed to characterize the crystal structure of the samples. Optical absorption spectra of the photoanodes between 350 nm and 900 nm were also recorded using a spectrophotometer (TU-1901).

The PEC performances of the photoanode were evaluated in a three-electrode configuration. The $BaSnO_3$ NWs-CdS QDs serve as the working electrode, saturated calomel electrode (SCE) is the reference electrode and platinum foil works as the counter electrode. The electrolyte was a mixed aqueous solution of 0.25 M Na_2S and 0.35 M Na_2SO_3 with a pH of 12.8. The illumination was provided by a 500 W Xe lamp equipped with an AM 1.5 G

Journal of Materials Chemistry A Accepted Manuscript

This journal is © The Royal Society of Chemistry [year]

filter. The incident photo intensity was calibrated to 100 mW cm^{-2} by a standard silicon solar cell.

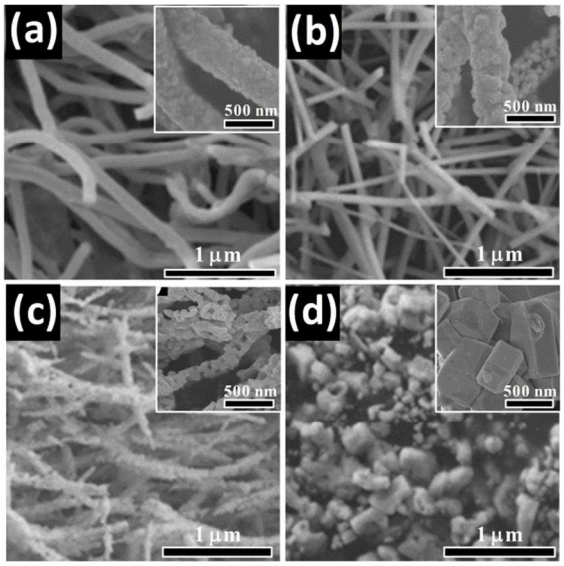

Fig. 2 The morphology evolution of the samples (11 wt.% PVP) as a function of calcination temperature. (a) 850 °C, (b) 900 °C, (c) 950 °C and (d) 1000 °C.

3. Results and discussion

Fig. 2 shows the morphology evolution of the $BaSnO_3$ NWs (PVP 11 wt.%) as a function of the calcination temperature. It is evident that the NWs calcined at 850 °C are consisted of numerous primary nanoparticles with an average diameter of 38.5 nm. When increasing the temperature, the average size of the primary nanoparticles increases. The sizes are 43.8 nm, 64.3 nm and 430 nm when calcined at typical temperature of 900 °C, 950 °C and 1000 °C, respectively. While the $BaSnO_3$ NWs tend to be broken at the high temperature.

The content of PVP also plays an important role on the formation of $BaSnO_3$ NWs. Fig. S1 shows the FESEM images of the $BaSnO_3$ NWs with PVP content of 9%, 11% and 13% in weight. All of the three samples were thermally treated at the same conditions. It is clear that the NWs stacked with nanoparticles become looser when the content of PVP increases. The nanoparticles in the NWs prepared from 11% PVP stacked more tightly, implying good inter-crystalline connections, which can facilitate fast electron transport and suppress charge recombination.

The crystallization degree of the pristine NWs (PVP content of 11 wt.%) influenced by calcination temperature are shown in Fig. 3 with XRD patterns. For the sample annealed at 850 °C, four diffraction peaks at 26.61°, 33.89°, 37.95° and 51.78° can be well indexed to the rutile structure of SnO_2 (JCPDS No. 41-1445), and the peaks at 30.69°, 43.96°, 54.56°, 63.91° and 72.56° indicate the emergence of cubic perovskite $BaSnO_3$ (JCPDS No. 15-0780). When the temperature rose to 900 °C, the characteristic peaks of SnO_2 almost disappeared, which indicated that the phase of cubic perovskite $BaSnO_3$ become dominant in this case. When continue to increase the temperature, the characteristic peaks of $BaSnO_3$ become much sharper, while a weak peak of SnO_2 (200) facet still exists in the products. This weak peak of SnO_2 (200) facet was believed to come from the FTO substrates, rather than the products.[16]

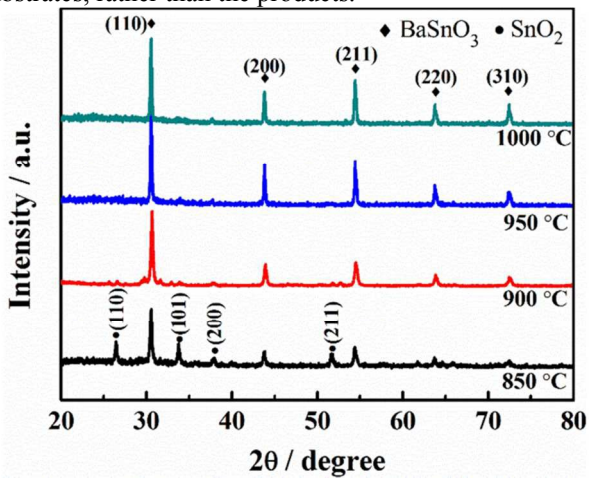

Fig. 3 Crystal structure of $BaSnO_3$ NWs influenced by the calcination temperatures.

In this work, the $BaSnO_3$ NWs prepared from the optimized precursor (11% PVP) and calcination temperature of 900 °C were selected for all the following investigation.

Further insight into the structural information was obtained by a TEM characterization on a single $BaSnO_3$ NW. As shown in Fig. 4a, the stacking of the nanoparticles is very tight and no obvious pores can be observed. The compact structure will promise a larger carrier mobility and lower charge recombination. Fig. 4b is an HRTEM image at a higher magnification, which shows well resolved lattice fringes even at the outer surface, indicating a high crystallinity of the NWs. The resolved spacing between two parallel adjacent fringes is about 0.21 nm, corresponding to the (200) plane of the cubic perovskite phase of $BaSnO_3$ (JCPDS No. 15-0780).[29]

To increase the light absorption in visible region, the $BaSnO_3$ NWs were decorated with CdS QDs by a SILAR method.[22] As shown in Fig. S2, after being decorated with CdS QDs for ten cycles, the surface of the NWs were coated with a layer of CdS nanoparticles uniformly, which is crucial to obtaining good PEC properties. SEM cross-sectional images of the CdS QD-decorated $BaSnO_3$ NWs on the fluorine-doped tin oxide (FTO) layer are

Journal of Materials Chemistry A Accepted Manuscript

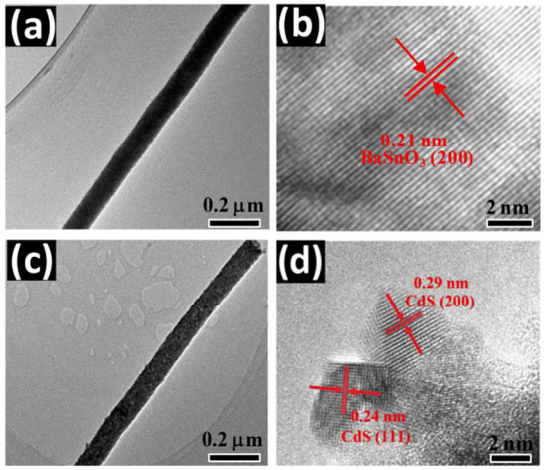

Fig. 4 TEM and HRTEM images of the $BaSnO_3$ NW (a), (b) and $BaSnO_3$ NW-CdS QDs (c), (d), respectively.

shown in Fig. S3. The NW structure of $BaSnO_3$ still can be clearly seen after CdS decoration. In addition, the film has a good adhesion with the FTO substrate, and there are no cracking or peeling-off, even the thickness of the films reaches up to 30 μm. The structural information of the CdS QD-decorated $BaSnO_3$ NWs was characterized by TEM. As shown in Fig. 4c, CdS QDs have an average size of 5 nm and uniformly distributed on the $BaSnO_3$ NW. Such a uniformly distribution of CdS QDs is attributed to the advantage SILAR method. In the second step of SILAR procedure, excess ions adsorbed on the substrate by Van-der Waals force will be removed by the rinse water, and the chemical reaction can only happen between the strongly specific adsorbed cations (Cd^{2+}) and the less strongly adsorbed anions (S^{2-}) adjacent to the nanowire surface. The uniform distribution of the QDs is attributed to the uniformly absorption of the ions in such a high temperature treated clean surface of the $BaSnO_3$ NWs. The loaded amount of CdS is about 0.2 mg after 10-cycle decoration when the amount of $BaSnO_3$ is 2 mg. The lattice spacing, 0.29 and 0.24 nm, in the HRTEM image (Fig. 4d) correspond to the (200) and (111) planes of CdS (JCPDS No. 80-0019), respectively. In order to further confirm the formation of CdS QDs on the fiber, the Cd and S elemental mapping has been performed. As shown in Fig.S4, the Cd (blue) and S (yellow) elements are homogeneously distributed on the surface of nanowire. This result implies that the CdS QDs are uniformly distributed on the $BaSnO_3$ nanowires' surface.

X-ray photoelectron spectra (XPS) were performed on the $BaSnO_3$ NWs-CdS QDs film to investigate its chemical compositions and electronic structures. Fig. 5a exhibits the survey spectrum, which including the peaks from Ba, Sn, O, Cd and S. Fig. 5b, c and d shows the O 1s, Cd 3d and S 2p core level XPS scanned at higher resolution over smaller energy windows, respectively. The O 1s XPS spectrum shows a peak with a binding energy of 573.1 eV. The Cd 3d core level XPS spectrum has two sharp peaks at 405.5 eV (Cd 3d 5/2) and 412.2 eV (Cd 3d 3/2) with a typical splitting energy of 6.7 eV, consisted with the previously reported values for CdS.[24] The S 2p core level spectrum given in Fig. 5d indicates that the S 2p has a doublet structure corresponds to S 2p 3/2 and 2p 1/2 orbitals of divalent sulfide ions (S2-) at 162.2 and 163.0 eV. Only a weak peak from oxidized form of sulfur (such as sulfate) was observed at 168.8 eV,[30] indicating that the CdS QDs were heat stable at 400 °C in short- time.

The light absorption of $BaSnO_3$ NWs and $BaSnO_3$ NWs-CdS QDs were determined by UV-vis absorption spectra (Fig. 6a). It can be seen that the $BaSnO_3$ NWs only absorbs UV light with correlation to its optical band gap (3.1 eV).[31] After decorated with CdS QDs, the absorption range of the photoanode has been extended to visible region with a maximum wavelength about 600 nm, indicating an effective usage of visible light. It's worth noting, that the band gap of pure CdS is 2.34 eV, and the

Journal of Materials Chemistry A Accepted Manuscript

This journal is © The Royal Society of Chemistry [year]

Cite this: DOI: 10.1039/c0xx00000x

www.rsc.org/xxxxxx

ARTICLE TYPE

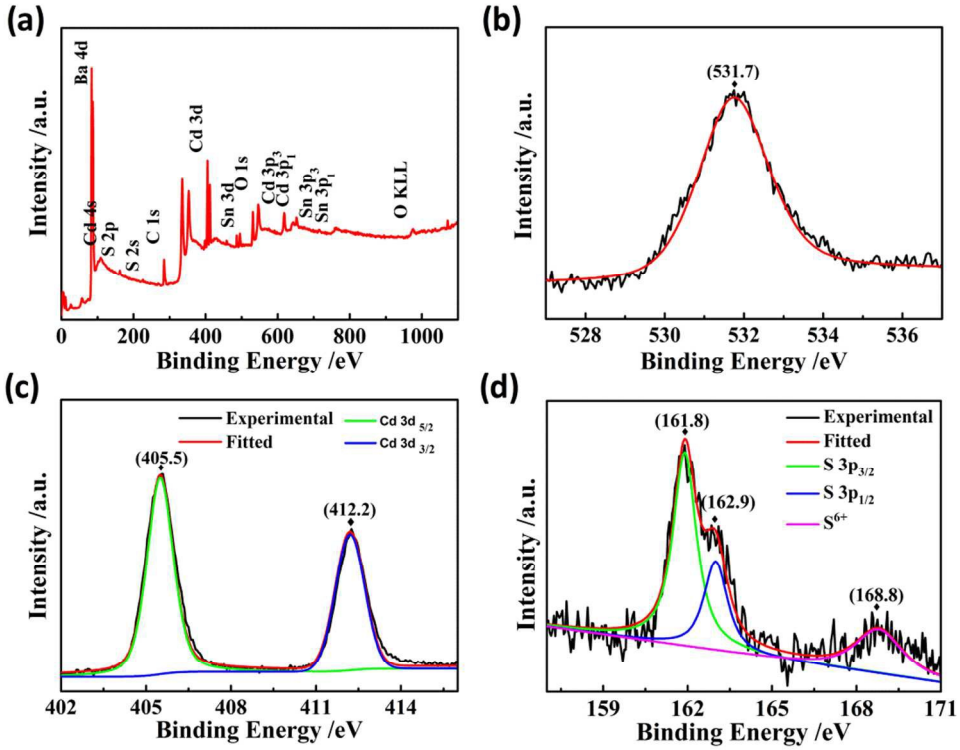

Fig. 5 (a) XPS fully scanned spectra of $BaSnO_3$ NWs-CdS QDs. High resolution XPS spectrum of O 1s (b), Cd 3d (c) and S 2p (d).

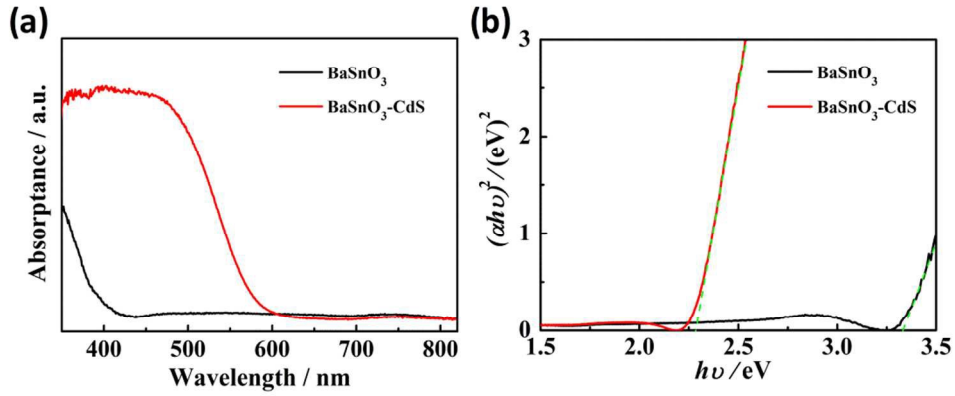

Fig. 6 (a) UV-vis absorption spectra and (b) the plots of band gap energy of pure $BaSnO_3$ NWs and $BaSnO_3$ NWs-CdS QDs.

absorption edge of pure CdS is around 530 nm in theory. However in Fig.6a, the hybrid $BaSnO_3$-CdS shows an absorption edge of 600 nm. Such a red shift of absorption edge may be attributed to the sulfide vacancies. It can be seen that there is a weak peak of S^{6+} in S 2p core level in the XPS spectrum (Fig. 6d). In general, point defects, such as sulfide vacancies and oxygen vacancies, are likely to narrow the band gap in many cases.[32] The relationship of the absorption coefficient and the incident photon energy of the semiconductor can be estimated by modified Kubelka–Munk function, as shown in Fig. 6b. It can be seen that CdS QD-decorated $BaSnO_3$ NWs have a slightly lower band gap (2.3 eV) than individual $BaSnO_3$ NWs (3.3 eV), which are very close to the reported value of CdS and $BaSnO_3$.[22, 26] These values demonstrated that the obtained $BaSnO_3$ NWs-CdS QDs samples exhibit a strong absorption in both UV and visible light.

As known, electrochemical impedance spectroscopy (EIS) can provide the interfacial information of photoanodes.[33] Fig. S5 shows the semicircular features of the photoanode/electrolyte

Journal of Materials Chemistry A Accepted Manuscript

interface Nyquist plots. The diameter of the semicircle equals to the electrical resistance *R* of photoanode/electrolyte interface, which controls the electron transfer kinetics of the redox probe. As shown in Fig S5, the arc diameter for the $BaSnO_3$/CdS heterostructures is much smaller than that of pristine $BaSnO_3$ nanowires, which indicates that the resistance *R* of $BaSnO_3$/CdS heterostructures is pretty lower than that of $BaSnO_3$ nanowires. This shows that such a heterojunction structure has effectively enhanced the electron mobility and suppressed the recombination of photoexcited electron-hole pairs in the $BaSnO_3$/CdS heterostructure photoanode. The reduced charge transfer resistance is believed to be a key factor for the improvement of PEC's performance.[34]

It is worth mentioning that the photocurrent going through an external circuit is widely used as a reliable surrogate for gas measurement in PEC hydrogen generation.[35-37] The hydrogen generation rate can be calculated from the photocurrent according to the following equation:

$$nH_2\ (\mu mol/(h\ cm^2)) = (1800 \times j\ (mA/cm^2) \times \eta_F) / (e(c) \times N_A)$$

j is the photocurrent density, η_F is the faradic efficiencies, *e(c)* is the electronic charge, and N_A is the Avogadro constant. More details about this equation can be found in supplementary materials.

In order to evaluate the PEC performance of $BaSnO_3$ NWs-CdS QDs photoanode, linear sweep voltammograms were measured in a three-electrode configuration with a solution containing 0.25 M Na_2S and 0.35 M Na_2SO_3 as electrolyte. The working area of the photoanode is about 0.4 cm^2. Fig. 7a displays a set of linear-sweep voltammograms of the $BaSnO_3$ NWs-CdS QDs photoanode with different decorating cycles. The dark current is almost zero through all the sweeping voltage. The $BaSnO_3$ NWs photoanode yields a photocurrent density of 0.5 mA cm^{-2} at 0 V versus SCE and photocurrent onset potential of -0.5 V vs. SCE under AM 1.5G (100 mW cm^{-2}) illumination. From Fig. 7b we can see, the photocurrent density drastically increased with the decoration cycle of CdS. When the decoration cycle is 10, it reached its maximum value of ~4.8 mA cm^{-2} (0 V vs. SCE) which corresponds to a hydrogen generation rate of 90 μmol (h $cm^2)^{-1}$ in theory by assuming $\eta_{F=1}$. However, η_F is always less than 1 in practical due to the existence of sacrificial agents. The maximum photocurrent is about nine times larger than that of the pure $BaSnO_3$ NWs. While further increasing the running cycles, the photocurrent density decreased sharply. It decreased to 2.5 mA cm^{-2} after 15 cycles. This phenomenon is in accordance with the reports of other groups,[22, 26, 38] which can be explained by the morphology change of the samples shown in Fig. S6. When the decorating cycle is less than 10, the amount of CdS QDs loaded on the surface of $BaSnO_3$ NWs increases with the decorating times, which facilitates photo absorption and generation of more electron-hole pairs. It is known that the ultrafast interfacial electron transfer and high-efficiency charge separation occurs only in the directly coupled QDs/semiconductor system.[39] Therefore, direct contact between CdS QDs and $BaSnO_3$ NWs is essential to obtain high PEC performance. However, as shown in Fig. S6c, further increase in the amount of CdS QDs results in the aggregation of the CdS QDs, which retards electron transfer from the indirectly-contact CdS QDs to $BaSnO_3$ NWs.[39, 40] The formation of big size CdS nanocrystals is another obstacle, which have poor ability to generate multiple excitons from the absorption of a single photon due to the disappearance of the quantum effect.[22] It is noteworthy that the changes in photocurrent onset potential give another advancement of the $BaSnO_3$ NWs-CdS QDs electrode. The photocurrent onset potential increased sharply from -0.5 V vs. SCE for $BaSnO_3$ NWs to -1.2 V vs. SCE for $BaSnO_3$ NWs-CdS QDs indicating much higher PEC activity of $BaSnO_3$ NWs-CdS

Journal of Materials Chemistry A Accepted Manuscript

This journal is © The Royal Society of Chemistry [year]

ARTICLE TYPE

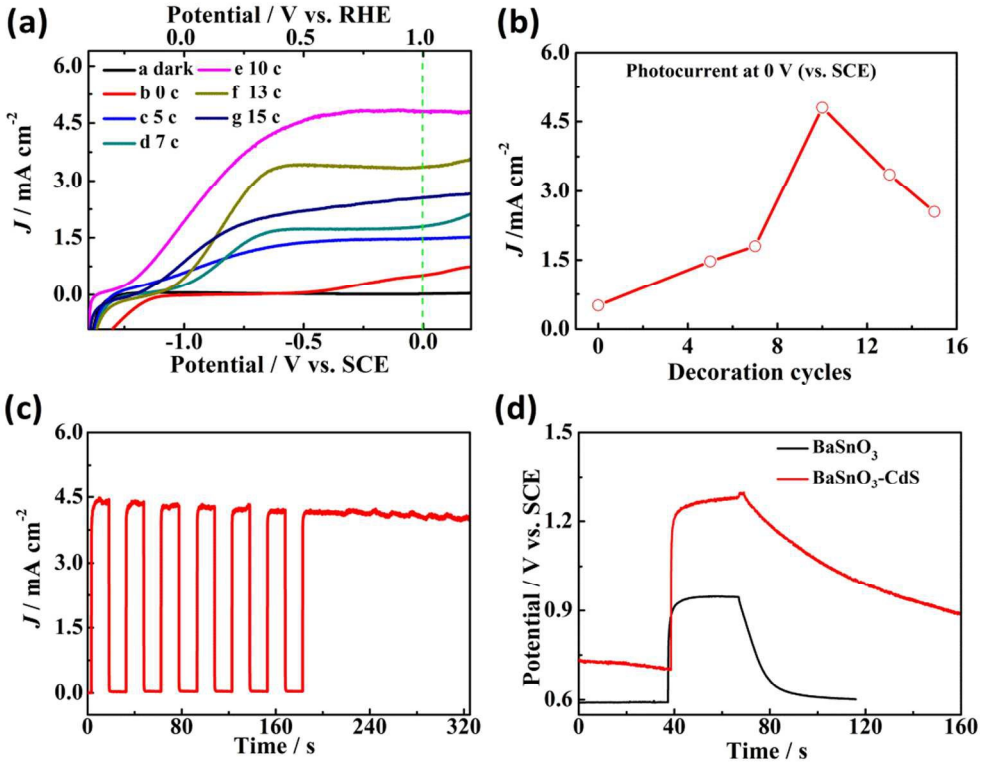

Fig. 7 (a) Linear-sweep voltammograms curves of $BaSnO_3$ NWs-CdS QDs with different decoration cycles. (b) Short-circuit photocurrent as a function of decoration cycles. Short-circuit photocurrent (c) and open circuit voltage (d) response of $BaSnO_3$ NWs-CdS QDs photoanode with on and off cycles.

QDs than that of $BaSnO_3$ NWs. Moreover, the recycle performance of the CdS QD-decorated $BaSnO_3$ photoanode was characterized in the three-electrode configuration. As shown in Fig. S7, the remained photocurrent was about 73% of the initial after 100 cycles.

Fig. 7c and d show the photoresponse of $BaSnO_3$ NWs-CdS QDs over time at 0 V vs. SCE for photocurrent (*J-t*) and at open circuit condition for voltage response (*V-t*) under pulsed light illumination. It can be seen that the photocurrent jumps sharply to ~4.0 mA cm^{-2} when the light is switched on, which indicates rapidly transferring of the photo-generated electrons from CdS QDs to $BaSnO_3$ NWs. In addition, the photocurrent decay rapidly to dark current once the light is switched off, indicating fast transport of photo-generated electrons in $BaSnO_3$ NWs. The *V-t* curves of $BaSnO_3$ NWs and $BaSnO_3$ NWs-CdS QDs were shown in Fig. 7d. The photovoltage for both of $BaSnO_3$ NWs and $BaSnO_3$ NWs-CdS QDs rises rapidly when the light was switched on and reached the saturation state within 10 s, which agrees with the rapid jump of the *J-t* curve. It is interesting that the photovoltage decay time (τ_d, defined as time to recovery to 1/e (37%) of the maximum photovoltage) of $BaSnO_3$ NWs-CdS QDs is more than 84 s, much larger than that of $BaSnO_3$ NWs (10 s), implying longer electron lifetime in $BaSnO_3$ NWs-CdS QDs than that in pure $BaSnO_3$ NWs. Such an increasing in electron lifetime is attributed to the contribution of $BaSnO_3$ NWs-CdS QDs heterojunction with type Ⅱ band alignment.[8] As show in Fig. 8, the conduction and valance band of CdS are both negative than that of $BaSnO_3$. The photoexcited electrons are transferred upon light irradiation from the CdS conduction band to the conduction band of $BaSnO_3$. The photoexcited holes accumulate on the valance band of CdS, thus reducing the recombination probability and increasing the lifetime of electrons [22]. Photoluminescence (PL) spectra analysis was also applied to reveal the functions of such a heterojunction formed at the $BaSnO_3$ /CdS interface. As shown in Fig. S8, the PL intensity of $BaSnO_3$ NWs was significantly decreased after being decorated with CdS QDs. This decrease can be attributed to the increased PL quenching, because of the enhanced electron transfer from CdS to $BaSnO_3$ by such a

Journal of Materials Chemistry A Accepted Manuscript

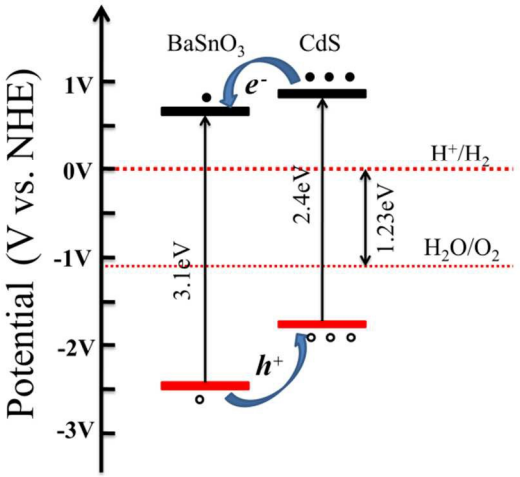

Fig. 8 A scheme of charge transfer mechanism in $BaSnO_3$ NWs-CdS QDs PEC photoanode.

favorable conduction band structure.[41]

IPCE is a valuable tool to provide insight into the PEC photo properties.[42] The IPCE measurements were carried out on typical photoanodes at 0 V (vs. RHE). As shown in Fig. S9, compared to $BaSnO_3$ the CdS QD-decorated $BaSnO_3$ showed a significantly enhanced photoactivity in the range of 350-550 nm. The results clearly confirm that the decoration of CdS QDS has effectively improved the visible-light absorption of $BaSnO_3$ NWs. Moreover, the heterojunction between CdS and $BaSnO_3$ will facilitate the charge separation and suppress the charge recombination, which greatly enhanced the IPCE.

The practical hydrogen generation rate has been quantified by gas chromatography. Fig. S10 shows the evolution of H_2 as a function of time under visible light irradiation and the bias is 0V (vs. SCE). The hydrogen generation rate is about 71.8 μmol (h cm^2)$^{-1}$ for the CdS QD-decorated $BaSnO_3$ photoanode, corresponding to a Faradaic efficiency around 80%.

4. Conclusions

In summary, highly crystalline $BaSnO_3$ NWs have been prepared by electrospinning from a precursor solution with a suitable mixed solvent. The optimized PVP content and annealing temperature are 11% and 900°C, respectively. After decorated with CdS QDs, the $BaSnO_3$ NWs yield remarkable photocurrent density of ~4.8 mA cm^{-2} at 0 V vs. SCE and a hydrogen generation rate of 71.8 μmol (h cm^2)$^{-1}$, corresponding to a Faradaic efficiency of close to 80%, which are nine times higher than that of $BaSnO_3$ NWs. Such a favorable PEC performance of the CdS QD-decorated $BaSnO_3$ NWs results from the high electron-hole generation rate at the CdS/$BaSnO_3$ interface and the low degree of charge recombination in the $BaSnO_3$ NWs during transport. The results indicate that CdS QD-decorated $BaSnO_3$ NWs is a promising candidate for high-efficient PEC water splitting, and the water splitting performance of PEC cells can be highly improved by rationally building interface band structures.

Acknowledgements

This work was partially supported by the National Natural Science Foundation of China (No. 61176058, 61404066), Science and Technology Planning Project of Sichuan Province (China, No. 2014JY0094) and the Scientific Research Foundation for the Returned Overseas Chinese Scholars, State Education Ministry of China.

Notes and references

[a] *School of Physical Science and Technology, Lanzhou University, Lanzhou 730000, China. Email: hanwh@lzu.edu.cn (Weihua Han); xieeq@lzu.edu.cn (Erqing Xie); Fax: (+86) 931 8913554; Tel: (+86) 931 8912616.*
[b] *Institute of Chemical Materials, China Academy of Engineering Physics, Mianyang 621900, China.*
‡ These authors contributed equally to this work.
†Electronic Supplementary Information (ESI) available:. See DOI:10.1039/b000000x/

References

1. M. Gratzel, *Nature*, 2001, **414**, 338-344.
2. A. Kudo and Y. Miseki, *Chem. Soc. Rev.*, 2009, **38**, 253-278.
3. M. G. Walter, E. L. Warren, J. R. McKone, S. W. Boettcher, Q. Mi, E. A. Santori and N. S. Lewis, *Chem. Rev.*, 2010, **110**, 6446-6473.
4. Z. Chen, T. F. Jaramillo, T. G. Deutsch, A. Kleiman-Shwarsctein, A. J. Forman, N. Gaillard, R. Garland, K. Takanabe, C. Heske, M. Sunkara, E. W. McFarland, K. Domen, E. L. Miller, J. A. Turner and H. N. Dinh, *J. Mater. Res.*, 2011, **25**, 3-16.
5. S. Y. Reece, J. A. Hamel, K. Sung, T. D. Jarvi, A. J. Esswein, J. J. H. Pijpers and D. G. Nocera, *Science*, 2011, **334**, 645-648.
6. H. Dotan, O. Kfir, E. Sharlin, O. Blank, M. Gross, I. Dumchin, G. Ankonina and A. Rothschild, *Nat Mater*, 2013, **12**, 158-164.
7. L. Gao, Y. Cui, J. Wang, A. Cavalli, A. Standing, T. T. Vu, M. A. Verheijen, J. E. Haverkort, E. P. Bakkers and P. H. Notten, *Nano Lett.*, 2014, **14**, 3715–3719.
8. R. Marschall, *Adv. Funct. Mater.*, 2014, **24**, 2421-2440.
9. Y. Qiu, S. F. Leung, Q. Zhang, B. Hua, Q. Lin, Z. Wei, K. H. Tsui, Y. Zhang, S. Yang and Z. Fan, *Nano Lett.*, 2014, **14**, 2123-2129.
10. P. Zhang, L. Gao, X. Song and J. Sun, *Adv. Mater.*, 2015, **27**, 562-568.
11. A. Fujishima and K. Honda, *Nature*, 1972, **238**, 37-38.
12. Q. Huang, F. Kang, H. Liu, Q. Li and X. Xiao, *J. Mater. Chem. A*, 2013, **1**, 2418-2425.
13. T. Jin, P. Diao, Q. Wu, D. Xu, D. Hu, Y. Xie and M. Zhang, *Appl. Catal. B: Environ.*, 2014, **148-149**, 304-310.
14. A. Kargar, Y. Jing, S. J. Kim, C. T. Riley, X. Pan and D. Wang, *ACS Nano*, 2013, **7**, 11112-11120.
15. C. W. Lai and S. Sreekantan, *Int. J. Hydrogen Energy*, 2013, **38**, 2156-2166.
16. Z. Liu, K. Guo, J. Han, Y. Li, T. Cui, B. Wang, J. Ya and C. Zhou, *Small*, 2014, **10**, 3153-3161.
17. J. Su, L. Guo, N. Bao and C. A. Grimes, *Nano Letters*, 2011, **11**, 1928-1933.
18. G. Wang, Y. Ling, D. A. Wheeler, K. E. George, K. Horsley, C. Heske, J. Z. Zhang and Y. Li, *Nano Lett.*, 2011, **11**, 3503-3509.
19. C. Cheng, Y. Y. Tay, H. H. Hng and H. J. Fan, *Journal of Materials Research*, 2011, **26**, 2254-2260.
20. X. Li, Z. Zhang, L. Chen, Z. Liu, J. Cheng, W. Ni, E. Xie and B. Wang, *Journal of Power Sources*, 2014, **269**, 866-872.
21. C. Han, Z. Chen, N. Zhang, J. C. Colmenares and Y.-J. Xu, *Adv. Funct. Mater.*, 2015, **25**, 221-229.
22. F. Su, J. Lu, Y. Tian, X. Ma and J. Gong, *Phys. Chem. Chem. Phys.*, 2013, **15**, 12026-12032.
23. G. Yang, W. Yan, Q. Zhang, S. Shen and S. Ding, *Nanoscale*, 2013, **5**, 12432-12439.
24. G. Yang, Q. Zhang, W. Chang and W. Yan, *J. Alloys Compd.*, 2013, **580**, 29-36.
25. H. Wang, S. Kalytchuk, H. Yang, L. He, C. Hu, W. Y. Teoh and A. L. Rogach, *Nanoscale*, 2014, **6**, 6084-6091.

Journal of Materials Chemistry A Accepted Manuscript

This journal is © The Royal Society of Chemistry [year]

26. S. S. Shin, J. S. Kim, J. H. Suk, K. D. Lee, D. W. Kim, J. H. Park, I. S. Cho, K. S. Hong and J. Y. Kim, *ACS Nano*, 2013, **7**, 1027-1035.
27. W. Zhang, J. Tang and J. Ye, *J. Mater. Res.*, 2011, **22**, 1859-1871.
28. C. Gao, X. Li, B. Lu, L. Chen, Y. Wang, F. Teng, J. Wang, Z. Zhang, X. Pan and E. Xie, *Nanoscale*, 2012, **4**, 3475-3481.
29. D. W. Kim, S. S. Shin, S. Lee, I. S. Cho, D. H. Kim, C. W. Lee, H. S. Jung and K. S. Hong, *ChemSusChem*, 2013, **6**, 449-454.
30. Y. Yin, Z. Jin and F. Hou, *Nanotechnology*, 2007, **18**, 495608.
31. H. Mizoguchi, H. W. Eng and P. M. Woodward, *Inorg. Chem.*, 2004, **43**, 1667-1680.
32. X. Li, C. Gao, J. Wang, B. Lu, W. Chen, J. Song, S. Zhang, Z. Zhang, X. Pan and E. Xie, *J. Power Sources*, 2012, **214**, 244-250.
33. C. Zhang, M. Shao, F. Ning, S. Xu, Z. Li, M. Wei, D. G. Evans and X. Duan, *Nano Energy*, 2015, **12**, 231-239.
34. M. Wu, W.-J. Chen, Y.-H. Shen, F.-Z. Huang, C.-H. Li and S.-K. Li, *ACS Appl. Mater. Interfaces*, 2014, **6**, 15052-15060.
35. Z. Zhang, R. Dua, L. Zhang, H. Zhu, H. Zhang and P. Wang, *ACS Nano*, 2013, **7**, 1709-1717.
36. T. Hamann, *Science*, 2014, **345**, 1566-1567.
37. J. Luo, J. H. Im, M. T. Mayer, M. Schreier, M. K. Nazeeruddin, N. G. Park, S. D. Tilley, H. J. Fan and M. Gratzel, *Science*, 2014, **345**, 1593-1596.
38. Y. J. Hwang, C. Hahn, B. Liu and P. Yang, *ACS Nano*, 2012, **6**, 5060-5069.
39. H. Tada, M. Fujishima and H. Kobayashi, *Chem Soc Rev*, 2011, **40**, 4232-4243.
40. H. Tada, T. Kiyonaga and S. Naya, *Chem. Soc. Rev.*, 2009, **38**, 1849-1858.
41. J. Yoo, S. Jeong, S. Kim and J. H. Je, *Adv. Mater.*, 2015, n/a-n/a.
42. X. Yang, A. Wolcott, G. Wang, A. Sobo, R. C. Fitzmorris, F. Qian, J. Z. Zhang and Y. Li, *Nano Lett.*, 2009, **9**, 2331-2336.

Journal of Materials Chemistry A Accepted Manuscript

TOC

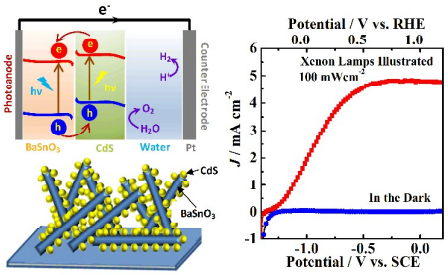

A staggered gap heterojunction has been built with $BaSnO_3$ nanowires and CdS quantum dots for high efficient water splitting photoanode.

Journal of Materials Chemistry A Accepted Manuscript